J Nanopart Res (2018) 20: 123
https://doi.org/10.1007/s11051-018-4226-2

BRIEF COMMUNICATION

Facile synthesis of three-dimensional diatomite/manganese silicate nanosheet composites for enhanced Fenton-like catalytic degradation of malachite green dye

De Bin Jiang · Yunsong Yuan · Deqiang Zhao · Kaiming Tao · Xuan Xu · Yu Xin Zhang

Received: 7 December 2017 / Accepted: 13 April 2018 / Published online: 29 April 2018

Abstract In this work, we demonstrate a novel and simple approach for fabrication of the complex three-dimensional (3D) diatomite/manganese silicate nanosheet composite (DMSNs). The manganese silicate nanosheets are uniformly grown on the inner and outer surface of diatomite with controllable morphology using a hydrothermal method. Such structural features enlarged the specific surface area, resulting in more catalytic active sites. In the heterogeneous Fenton-like reaction, the DMSNs exhibited excellent catalytic capability for the degradation of malachite green (MG). Under optimum condition, 500 mg/L MG solution was nearly 93% decolorized at 70 min in the reaction. The presented results show an enhanced catalytic behavior of the DMSNs prepared by the low-cost natural diatomite material and simple controllable process, which indicates their potential for environmental remediation applications.

Keywords Diatomite · Manganese silicate · Three-dimensional nanostructures · Fenton-like reaction · Catalytic applications

Electronic supplementary material The online version of this article (https://doi.org/10.1007/s11051-018-4226-2) contains supplementary material, which is available to authorized users.

D. B. Jiang · K. Tao · Y. X. Zhang (✉)
State Key Laboratory of Mechanical Transmissions, College of Materials Science and Engineering, Chongqing University, Chongqing 400044, People's Republic of China
e-mail: zhangyuxin@cqu.edu.cn

Y. Yuan · D. Zhao · X. Xu (✉)
Key Laboratory of Three Gorges Reservoir Region's Eco-Environment, Ministry of Education, Chongqing University, Chongqing 400045, China
e-mail: xuxuan@cqu.edu.cn

Introduction

Massive synthetic organic contaminants, including dyes, antibiotics, and industrial chemicals, threaten human health by discharging into the aquatic environment without treatment. Many methods, such as adsorption, extraction, and biological treatment, are used to remove the organic contaminants before discharging into natural environment (Fu et al. 2016; Liu et al. 2014; Ventura-Camargo Bde et al. 2016). Recently, the application of advanced oxidation processes (AOPs) based on heterogeneous Fenton-like catalysis is an attractive option for the removal of the organic contaminants (Jiang et al. 2018; Subramanian and Madras 2016). In particular, manganese-based compounds with the peculiar properties including abundant existence, environmental benignity, facile fabrication, and low cost have been regarded as a promising heterogeneous Fenton-like catalyst toward the degradation reaction due to the remarkably versatile redox chemistry of Mn (Bai et al. 2016; Zhang et al. 2014a). Considerable efforts have been devoted to fabricating manganese-based nanomaterials as Fenton-like catalyst, such as Mn_3O_4, MnO_2, MnOOH, and $MnSiO_3$ (Chen and He 2008; Yin et al. 2010; Zhan et al. 2015). However, their catalytic performance is still inefficient probably due to lack of surface active sites and long electron diffusion pathways,

limiting the improvement of the catalysis efficiency. Thus, it is desirable to explore the catalysts, which have a high specific surface area and porosity.

To address this issue, the use of solid materials as supports for immobilization of manganese-based nanomaterials seems to be of practical significance because it can inhibit the aggregation of neighboring nanoparticles to expose more effective surface active sites (Lee et al. 2016; Zhang et al. 2014c). Meanwhile, three-dimensional (3D) porous architectures attracted significant attention owing to their high specific surface area, fine-defined interior voids, low density, and good permeation property, which could significantly enhance catalyst loading, enlarge contact area, and shorten electron diffusion pathways in the catalysis (Berruyer et al. 2017; Yu et al. 2017). For instance, Zeng and co-workers (Yec and Zeng 2014) showed the manganese silicate nanospheres supported by silica spheres with nanobubble-shell 3D structure, exhibiting an ideal effective decomposition of dyes. Gao and co-workers (Gao et al. 2017) studied the preparation of $MnSiO_3$ 3D mesoporous silica spheres and its promising application in environmental remediation; the as-prepared $MnSiO_3$ 3D structure nanomaterials showed a good ability to remove pollutant in waste water. However, the preparation procedures of the sophisticated 3D porous support materials are always complicated and the cost of that is expensive, which severely hampers the further applications.

Diatomite is a kind of natural material with complex 3D architectures, which is typical of natural siliceous rocks containing mass of the amorphous silica (Li et al. 2015). Their hollow pill-box structure, large inner space with micro- and nano-scale porosity, high surface area, chemical inertness, low cost, nontoxicity, and low-density biogenetic sediment make diatomite a promising material for many applications (Guo et al. 2016; Le et al. 2017; Zhang et al. 2014b). It is not surprising that these unique 3D structures with combination of macro- and mesoporosity have been considered as a promising carrier and template to overcome the shape challenges of many synthetically prepared catalyst for environmental remediation (Yuan et al. 2016). Moreover, the amorphous silica on the surface of diatomite makes it an excellent nonmetallic template, since SiO_2 has been explored as a familiar one in self-assembly hard template method, especially important in fabricating nanomaterials.

Hence, in this study, we proposed a facile surfactant-free approach for fabricating 3D structure diatomite decorated by manganese silicate nanoparticles with controllable morphology using a hydrothermal method. Furthermore, the application of the optimum diatomite/manganese silicate nanosheets as Fenton-type catalysts for degradation of the MG dye was investigated. The diatomite/manganese silicate nanosheets (DMSNs) exhibited prominent ability for degradation of the MG dye from contaminated water.

Experimental section

Synthesis of diatomite/$MnSiO_3$ (DMSNs)

All chemicals were of analytical-reagent quality and were used without further purification. In a typical synthesis, 153 mg of $MnSO_4 \cdot H_2O$ and 200 mg of sodium maleate were dissolved in 20 mL of deionized water at room temperature. After stirring for about 20 min, 50 mg of purified diatomite was added to the above solution, stirring for another 20 min to form a homogeneous suspension at pH 8.2. The mixture was transferred into a 50-mL Teflon-lined stainless steel autoclave maintained at 180 °C for hours. After heating, the autoclave was cooled naturally to room temperature. Finally, the product was washed with deionized water and ethanol for times and dried at 60 °C to yield the DMSNs. The DMSNs prepared for 6 and 12 h were designated as DMSNs-1 and DMSNs-2, respectively.

Material characterization

The morphological and energy dispersive spectrometer analyses were examined on a focused ion beam (Zeiss Auriga FIB/SEM). The powder X-ray diffraction (XRD) patterns were collected on an X-ray diffractometer (D/max 2500, Cu Kα) with scattering angles. The functional groups in the sample were measured by Fourier transform infrared (FT-IR) spectroscope (Nicolet), where the spectra were performed in KBr pellets and recorded in the spectral region from 4000 to 400 cm^{-1}. The N_2 adsorption/desorption analysis was performed on a micromeritics instrument (ASAP 2020) at 77 K, and the pore size distributions were calculated from the adsorption branch by the Barrett–Joyner–Halenda (BJH) method. The X-ray photoelectron spectra (XPS) were detected by an X-ray photoelectron spectrometer (ESCALAB250Xi) using Al Kα X-ray as the radiation

source. The binding energy scale was calibrated which referred to carbon 1s peak at 284.6 eV.

Fenton-like degradation experiments

The catalytic performance of DMSNs was evaluated by the oxidative degradation of MG dye via a Fenton-like chemical reaction. Typically, 100 mL of MG solution (500 mg/L) was prepared in a 250-mL glass beaker under a fixed temperature of 30 °C. Then, 30 mg of DMSNs was added into the above solution with constant magnetic stirring (around 550 rpm) for 30 min to reach absorption–desorption equilibrium. Subsequently, H_2O_2 was added to the obtained suspension. At predetermined time intervals, a 4 mL suspension was withdrawn and the solid catalyst was separated immediately from the solution by centrifugation. The concentrations of MG in the course of degradation were measured at the maximum absorption wavelength (617 nm) by using the UV–vis spectrophotometer (Shimadzu, UV-2450).

Results and discussion

Structure and morphology

The overall fabrication process of 3D DMSNs involves three main steps, as illustrated in Scheme 1. First, a small portion of the SiO_2 phase from the surface of diatomite is hydrolyzed in situ to form H_4SiO_4, and at the same time, surface active sites are generated for the adsorption of Mn carboxylate species. Second, the active sites and Mn^{2+} decrease the activation energy for decomposition of the carboxylate. Then, the carboxylate groups decompose into CO_2 which serves as a soft template for the deposition of manganese silicate through ion exchange of Mn^{2+} with H_4SiO_4 (Yec and Zeng 2014). Third, these reactions would continue to form a thin film of porous manganese silicate nanosheet coating on the surface of diatomite during the thermal treatment process. Meanwhile, the solution pH decreased from 8.2 to 7.1 and 6.2 after the 6- and 12-h hydrothermal process, respectively, indicating that more H^+ ions were formed in the solution due to the exchange of Mn^{2+} with H_4SiO_4.

The typical X-ray diffraction (XRD) patterns of the diatomite, DMSNs-1, and DMSNs-2 are presented in Fig. 1. It can be seen from the curve of the diatomite that the diffraction peaks at 2θ of 21.9, 28.4, 31.4, 36.1, 42.6, 44.8, 47.0, 48.6, and 57.1° are in good agreement with the standard pattern of the SiO_2 phase (JCPDS card no. 39-1425), corresponding to (101), (111), (102), (200), (211), (202), (113), (212), and (301) planes (Zhang et al. 2014d). The diffraction peaks from DMSNs-1 and DMSNs-2 at 18.0, 28.9, 32.3, 38.1, 44.2, 50.7, 58.4, and 59.8° are in clear accordance with the standard pattern of the manganese silicate phase (JCPDS card no. 12-0181); meanwhile, the peaks attributed to the diatomite are obviously discovered in the patterns of the DMSNs-1 and DMSNs-2. It indicates the existences of diatomite and $MnSiO_3$ (Ling et al. 2016), and that the surface of diatomite is coated with $MnSiO_3$, which is in accordance with the initial design.

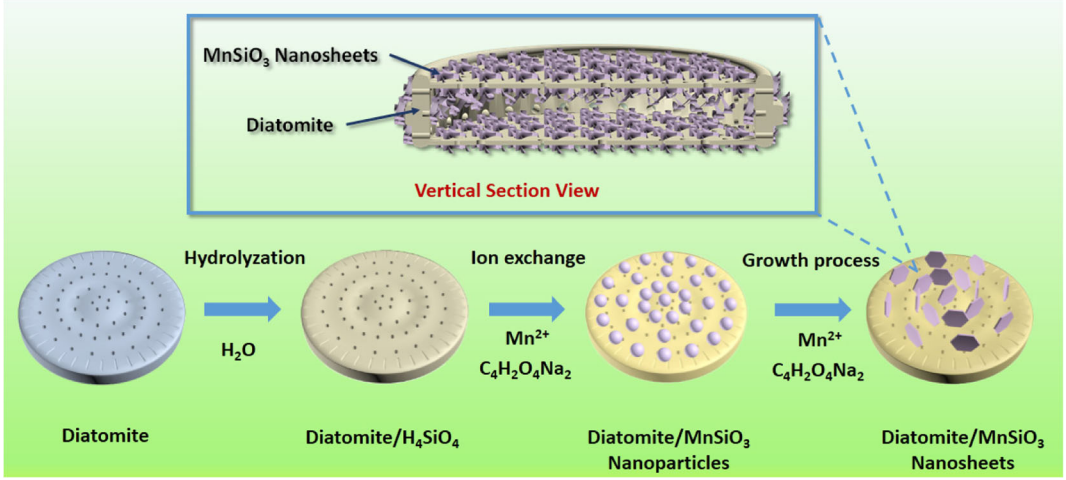

Scheme 1 Schematic illustration of the growth mechanism of the DMSNs

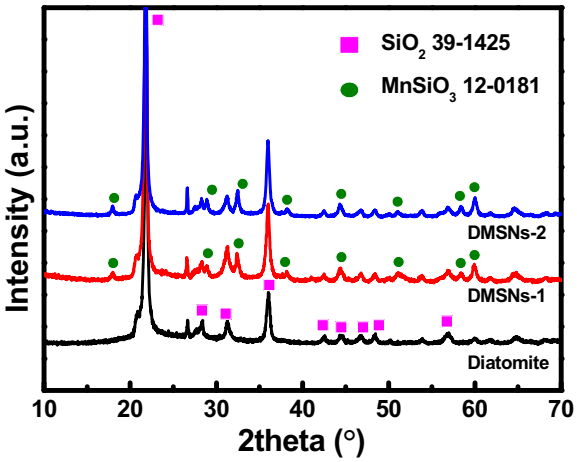

Fig. 1 XRD patterns of diatomite, DMSNs-1, and DMSNs-2

The scanning electron microscope (SEM) demonstrates the morphology of the samples. Figure 2 shows the SEM images of the diatomite and the DMSN samples obtained after hydrothermal treatments for 6 and 12 h, respectively. In Fig. 2a, the original diatomite presents porous disk-like shape with a diameter of circa 20 μm. As precisely observed from Fig. 2b, the surface of the original diatomite is relatively smooth. The comparative SEM images of DMSN samples in Fig. 2c, e exhibit a fairly rough surface and coating layer, which reveals that the $MnSiO_3$ were in situ reaction on the surface of diatomite with directional growth process. After 6 h of hydrothermal treatments, the $MnSiO_3$ on the surface of DMSNs-1 exhibits monodisperse, uniform, and spherical morphologies from the high-magnification SEM image in Fig. 2d. With the additional hydrothermal time from 6 to 12 h, as shown in Fig. 2e, a thicker layered film composed of $MnSiO_3$ is uniformly grown on the diatomite to form a coating on the surface. Moreover, the higher magnification SEM image in Fig. 2f reveals that the $MnSiO_3$ nanosheet morphology was formed from a small particle structure. The $MnSiO_3$ nanosheets with means of size 50 nm are interconnected with each other to form a very thin porous framework on diatomite, which is important for their function for proposed 3D composite. As seen from the SEM images of broken DMSNs-2 (Fig. S1), it is also confirmed that $MnSiO_3$ nanosheets are deposited inside the pores and inside the diatomite structures, which demonstrates that the modification process occurred on both internal and external diatomite surface. To reconfirm the mass percentage of $MnSiO_3$ in the DMSNs of varied treatment time, the samples were analyzed by EDS, as shown in Fig. (S2). The EDS elemental mapping confirms that the presence of Mn wt% increases from 9.68 to 12.59%, which means the mass percentage of $MnSiO_3$ in the DMSNs-1 and DMSNs-2 is estimated to be 17.6 and 22.9%, respectively. Such uniformly grown and higher loading capacity of $MnSiO_3$ is propitious to improve the Fenton-like catalytic reaction by providing rich active sites.

The porosity and pore structure parameters of the original and the $MnSiO_3$-modified diatomite were confirmed by nitrogen adsorption desorption isotherm and BJH pore size distribution. Upon the deposition of $MnSiO_3$ onto the diatomite, the specific surface area and pore volume increases evidently from circa 1.19 $m^2 \cdot g^{-1}$ and 0.0022 $m^3 \cdot g^{-1}$ for the original diatomite to circa 36.93 $m^2 \cdot g^{-1}$ and 0.0411 $m^3 \cdot g^{-1}$ for the DMSNs-2, respectively (Table 1). This results indicate the slowly growth of $MnSiO_3$ nanosheets on the surface of diatomite need time to effectively deposit on the surface areas of the diatomite. As shown in Fig. 3a, the H_3-type hysteresis loop in the isotherm of DMSNs-1 and DMSNs-2 caused by the slit-shaped pores resulting from aggregates of plate-like particles grows larger with the increasing reaction time, which also indicates the formation of the $MnSiO_3$ nanosheet morphology. The type IV isotherm of DMSNs-2, together with a capillary condensation step in the relative pressure range from 0.4 to 0.9, indicates that the DMSNs-2 is representative of large-pore mesopore structure (Dong et al. 2014). The prepared DMSNs-2 with more mesoporous structure can promote diffusion of reactants and products, which is beneficial to acquire a higher catalytic activity. Seeing the pore size distributions of the diatomite, DMSNs-1 and DMSNs-2 from Fig. 3b, it is noted that the synthesized $MnSiO_3$ nanosheets have a widen pore size distribution with the range of around 10 nm, which might be beneficial for the adsorption and mass transfer in the liquid system. These results further demonstrate that the high surface area and porous channels of DMSNs-2 should enhance catalytic performance by providing more reaction sites and facilitating the diffusion of pollutant and product into/out of the catalyst.

The surface properties of the DMSNs-2 are the main factors for the degradation of organic pollutions in heterogeneous catalytic Fenton reaction (Zhang et al. 2016b). The FTIR spectrum of the DMSNs-2 is shown in Fig. 4a. The absorbance at 1086 cm^{-1} is ascribed to the Si–O bond (Xiao et al. 2016). Two peaks at 790 and 477 cm^{-1} correspond to the symmetrical stretching vibrations of Si–O–Si

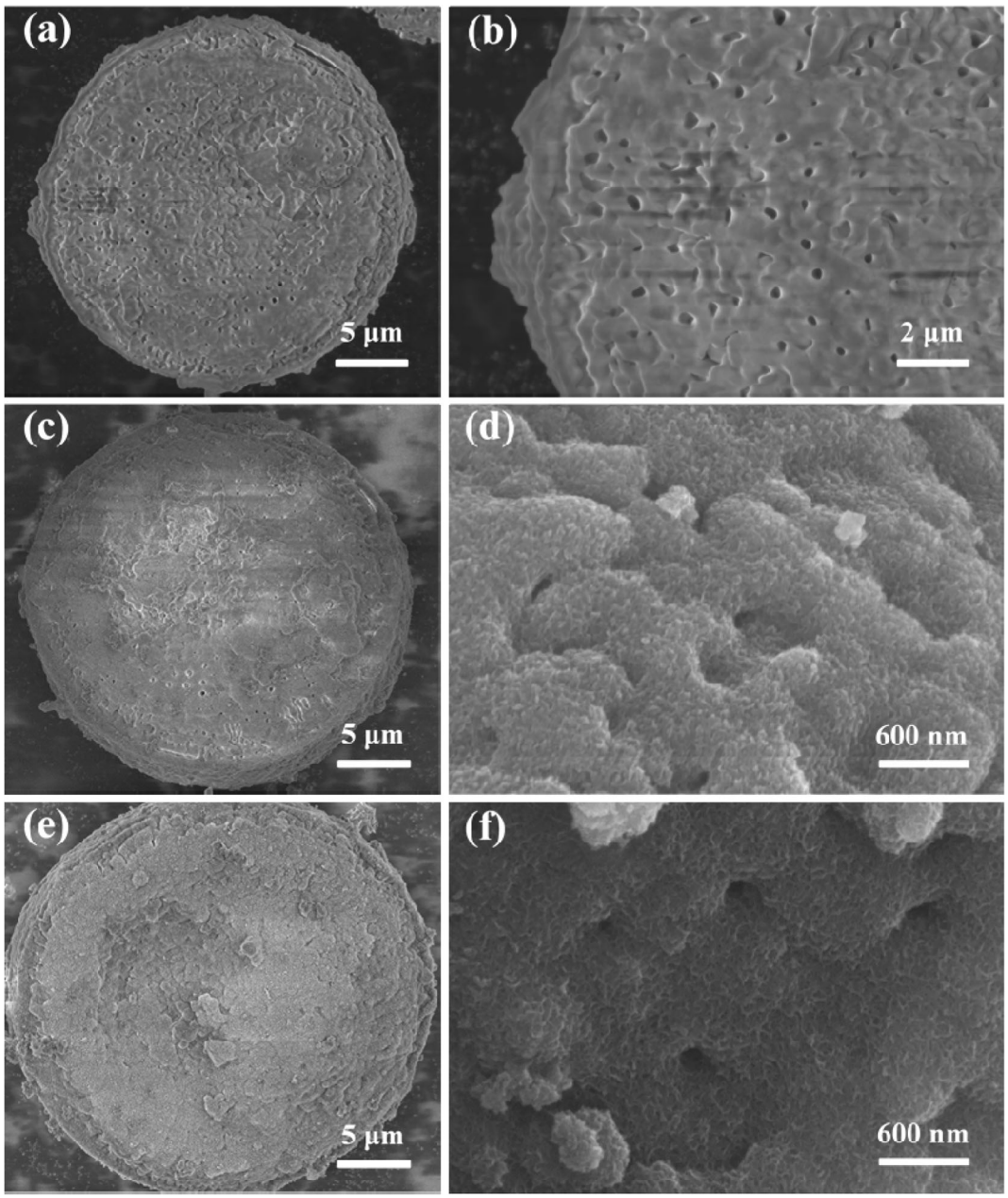

Fig. 2 SEM images of **a**, **b** diatomite; **c**, **d** DMSNs-1; and **e**, **f** DMSNs-2

Table 1 Surface area features determined from BET analysis for the diatomite, DMSNs-1, and DMSNs-2 samples

Samples	Specific surface area ($m^2 \cdot g^{-1}$)	Pore volume ($m^3 \cdot g^{-1}$)	Pore size (nm)
Diatomite	1.1855	0.002167	8.2391
DMSNs-1	24.6326	0.030846	5.0541
DMSNs-2	36.9292	0.041066	4.8316

bond and symmetrical stretching vibration of Si-O bond (Gao et al. 2015). The peak at 620 cm^{-1} is attributed to the lattice vibration of Mn–O bond, further confirming the growth of manganese silicate (Hao et al. 2016). The peak around 3439, 1579, and 1392 cm^{-1} is ascribed to the hydrogen-bonded hydroxyl groups of adsorbed water molecules, the bending vibration of absorbed water and the

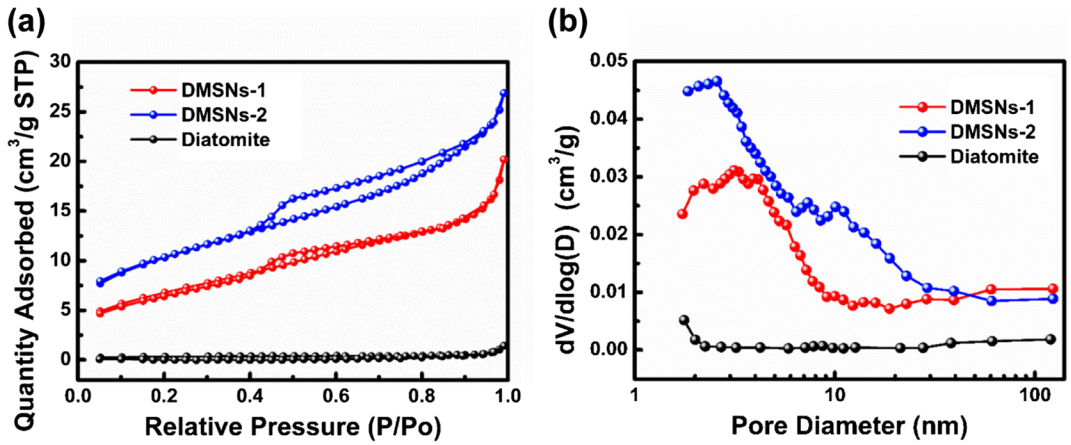

Fig. 3 **a** The nitrogen adsorption–desorption isotherms and **b** the corresponding pore size distribution curves of diatomite, DMSNs-1, and DMSNs-2

deformation vibrations of Mn–OH, respectively (Shang et al. 2016). These surface hydroxyl groups have advantages over catalytic Fenton reaction and catalytic decomposition.

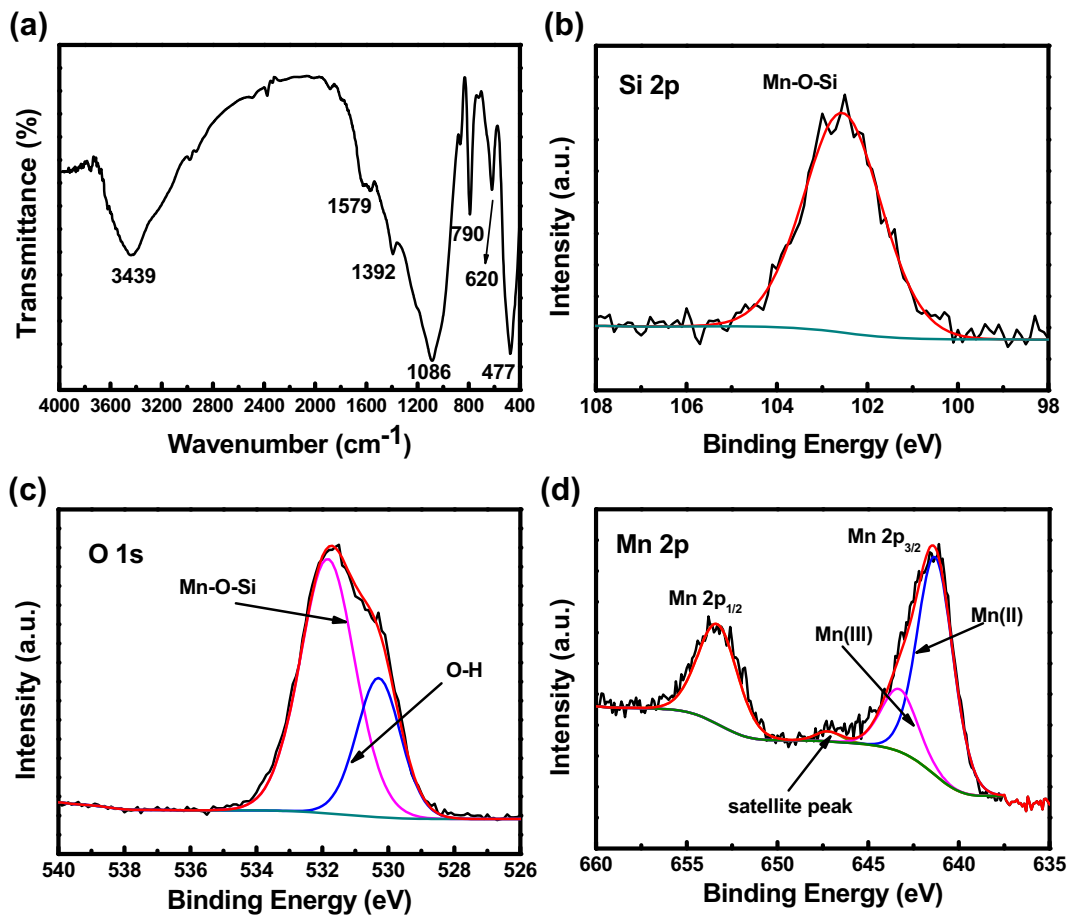

Fig. 4 **a** FT-IR spectra of DMSNs-2; **b** Si 2p; **c** O 1s; and **d** Mn 2p XPS spectra of DMSNs-2

The surface element composition of the DMSNs-2 was further investigated by XPS measurement. As shown in Fig. 4b, the binding energies at 102.6 eV was attributed to the Si 2p from Mn–O–Si, which is lower than that of the Si 2p in pure SiO_2 (Qu et al. 2012). In Fig. 4c, the O 1s spectra exhibit asymmetric peaks, indicating the existing of different degrees of oxygen contribution on the DMSNs-2 surface. The O 1s peaks could be deconvoluted into two peaks, with the binding energies at 531.8 and 530.2 eV corresponding to Mn–O–Si and O–H respectively (Zhang et al. 2016c). The Mn 2p3/2 peaks were fitted into two curves in Fig. 4d. The binding energies at 641.3 and 643.2 eV were indexed to Mn(II) and Mn(III) (Zhang et al. 2016c). The Mn 2p1/2 peak is found at 653.3 eV. The peaks at 647.2 eV are the satellite peak of Mn 2p (Zhu et al. 2018). The presence of the satellite peak reflects the occurrence of Mn(II) (Tan et al. 2016). In this Fenton reaction process, the electrons from the surface Mn(III) or Mn(II) induce H_2O_2 decomposition to active hydroxyl radical to degrade pollutant. Thus, it is expected that DMSNs-2 with rich versatile manganese valence could probably exhibit the promising catalytic properties in Fenton system.

Fenton-like catalytic degradation of malachite green

The potential absorptive and catalytic properties of the as-synthesized DMSNs-2 in environmental remediation at different systems were evaluated. The variation of MG concentration with time was presented in Fig. 5a. As seen in Fig. 5a, the H_2O_2 can hardly oxidize MG in absence of catalysts in 70 min. When the original diatomite was used as a catalyst, the degradation efficiency of MG is less than 10% in 70 min. When the original diatomite and the DMSNs-2 were used as adsorbents in absence of H_2O_2, the concentration of MG rapidly decreased within 20 min and the degree of decoloration holds at 3 and 20% respectively with increasing reaction time. These results indicate the loading of $MnSiO_3$ on

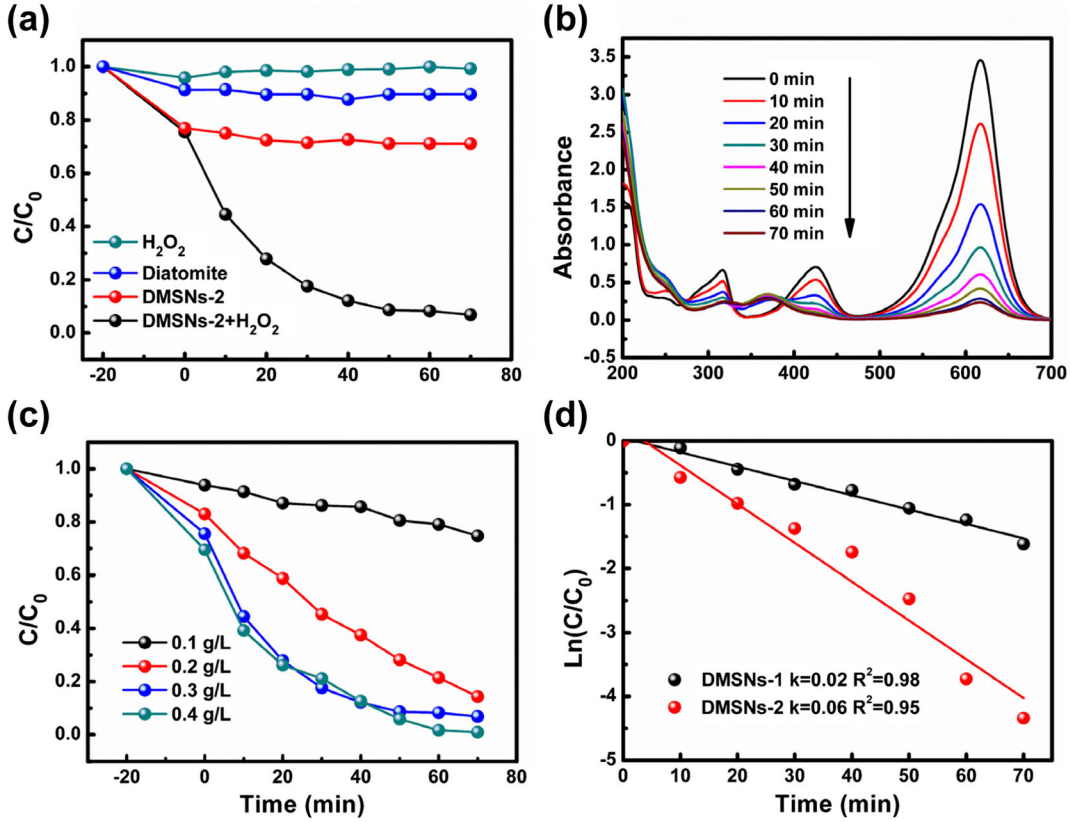

Fig. 5 **a** MG degradation under Fenton-like catalytic reaction condition; **b** UV-vis spectral changes for MG degradation with DMSNs-2/H_2O_2 system (reaction condition [MG] = 500 mg/L, [catalysts] = 0.3 g/L, [H_2O_2] = 30 mM); **c** MG degradation under different catalyst dosage conditions (reaction condition [MG] = 500 mg/L,, [H_2O_2] = 30 mM); **d** Plots of Ln(C/C_0) versus time for the catalytic reaction of DMSNs-1and DMSNs-2

the diatomite supplies highly absorptive properties of MG molecules due to large specific surface area of DMSNs-2, which should be also favorable of the catalytic decomposition of MG. Upon further addition of H_2O_2 oxidant into the MG- and DMSNs-2-mixed solution, the decoloration of MG was promoted, while the DMSNs-2 was employed as a heterogeneous Fenton catalyst in this system. The resultant solution can be decolored by 70% in 30 min and 93% in 70 min. These results suggest that the MG decoloration is caused by DMSNs-2 absorption and then H_2O_2-induced oxidation catalyzed by the DMSNs-2. To understand and clarify the changes in molecular structure of MG in the presence of DMSNs-2/H_2O_2 system, UV-vis spectra changes in the dye solution over various time intervals are shown in Fig. 5b. Clearly, the main absorption peak of MG molecules locating at 617 and 424 nm decreases rapidly with extension of the exposure time. Further exposure leads to no absorption peak at 617 nm in the whole spectrum. Besides, new absorption peak at 334 nm was observed with increasing the exposure time, which indicates the complete catalytic degradation of MG, and the generation of intermediate products. As seen in Fig. 5c, an increase of the DMSNs-2 dosage from 0.1 to 0.3 g/L could enhance the MG degradation efficiency. However, further increasing the DMSNs-2 dosage did not improve the degradation efficiency significantly. It showed that the overdose of catalyst could not further greatly improve the degradation efficiency of MG with the limited amount of H_2O_2 in the system

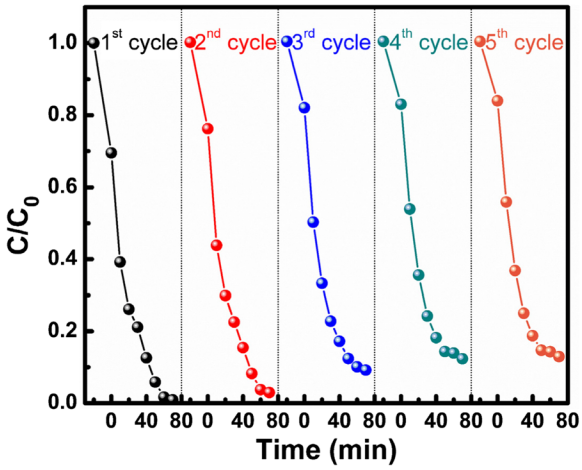

Fig. 6 Recycled performance of DMSNs-2 for degradation of malachite green dye under Fenton-like reaction. (reaction condition [Malachite green] = 500 mg/L, [catalysts] = 0.3 g/L, [H_2O_2] = 30 mM)

(Zhang et al. 2016a). Therefore, considering the economic factor, the right catalyst amount should be adopted in the real applications. The kinetics of MG degradation as a function of DMSNs-1 and DMSNs-2 catalyst were investigated. According to the results (Fig. 5d), the MG degradation reaction of the both DMSNs-1 and DMSNs-2 catalyst followed pseudo-first-order kinetics. In comparison, the DMSNs-2 catalyst leads to higher reaction rate constant. The enhancement of the kinetic rate may be attributed to the increasing reactive sites from higher exposed surface areas and more porous structure. These results reveal that the DMSNs-2 is a fairly catalyst in the Fenton-like reaction and is a hopeful catalyst in the practical applications.

The reusability of a catalyst is a key factor for its application. Therefore, it is necessary to investigate the reusability of the DMSNs-2 from the economic and environmental perspective. In this study, the DMSNs-2 was separated by a simple centrifugation and reused without further treatment after each cycle experiment. As shown in Fig. 6, the DMSNs-2 shows very fine repeatability in the first two rounds. Afterwards, the DMSNs-2 exhibits little loss of catalytic activity in the last three rounds but still keeps almost 90% catalytic activity. This drop could be attributed to the less activated site due to the coverage of area by intermediate products. Conclusively, the DMSNs-2 shows well recyclability.

Conclusion

In summary, the fabrication of novel 3D porous architecture manganese silicate nanosheet catalyst supported on natural diatomite structures is demonstrated. The analysis of the structure and morphology confirms that manganese silicate nanoparticles are uniformly grown on the inner and outer surface of diatomite, which significantly enlarges the specific surface area and porosity. The DMSNs used as a heterogeneous Fenton-like catalyst exhibited excellent catalytic activity in degradation of MG dye from an aqueous solution. The use of DMSNs resulted in nearly 93% of decolorization of 500 mg/L MG dye at 70 min of reaction under best conditions. Owing to simplicity and low cost of presented synthetic approach based on natural diatomite material, these results indicate evident potential diatomite-based composites for environmental remediation applications.

Acknowledgements The authors would like to extend special thanks to Ms. Qian Chen of Chongqing University for language polishing and Mr. Tianxu Zheng of Chongqing University for presentation of the scheme and figures modifying. The authors also thank the Electron Microscopy Center of Chongqing University for material characterizations.

Funding information The authors gratefully acknowledge the financial support provided by the State Education Ministry and Fundamental Research Funds for the Central Universities (106112017CDJXSYY0001, 106112016CDJZR135506, 106112017CDJQJ138802 and 106112017CDJSK04XK11), the National Natural Science Foundation of China (Grant no. 21576034), Chongqing University Postgraduates' Innovation Project (No. CYB16014 and CYS17003), and the Innovative Research Team of Chongqing (CXTDG201602014).

Compliance with ethical standards

Conflict of interest The authors declare that they have no conflict of interest.

References

Bai B, Qiao Q, Arandiyan H, Li J, Hao J (2016) Three-dimensional ordered mesoporous MnO_2-supported ag nanoparticles for catalytic removal of formaldehyde. Environ Sci Technol 50:2635–2640. https://doi.org/10.1021/acs.est.5b03342

Berruyer P, Lelli M, Conley MP, Silverio DL, Widdifield CM, Siddiqi G, Gajan D, Lesage A, Copéret C, Emsley L (2017) Three-dimensional structure determination of surface sites. J Am Chem Soc 139:849–855. https://doi.org/10.1021/jacs.6b10894

Chen H, He J (2008) Facile synthesis of monodisperse manganese oxide nanostructures and their application in water treatment. J Phys Chem C 112:17540–17545. https://doi.org/10.1021/jp806160g

Dong F, Ou M, Jiang Y, Guo S, Wu Z (2014) Efficient and durable visible light photocatalytic performance of porous carbon nitride nanosheets for air purification. Ind Eng Chem Res 53:2318–2330. https://doi.org/10.1021/ie4038104

Fu Y, Wei Q, Lu B, Wang X, Sun S (2016) Stem-like nano-heterostructural MWCNTs/α-Fe_2O_3?@TiO_2? composite with high lithium storage capability. J Alloys Compd 684:419–427. https://doi.org/10.1016/j.jallcom.2016.05.185

Gao Y, Wang Y, Zhang H (2015) Removal of rhodamine B with Fe-supported bentonite as heterogeneous photo-Fenton catalyst under visible irradiation. Appl Catal B Environ 178:29–36. https://doi.org/10.1016/j.apcatb.2014.11.005

Gao Q, Li HT, Ling Y, Han B, Xia KS, Zhou CG (2017) Synthesis of $MnSiO_3$ decorated hollow mesoporous silica spheres and its promising application in environmental remediation. Microporous Mesoporous Mater 241:409–417. https://doi.org/10.1016/j.micromeso.2016.12.026

Guo XL, Kuang M, Li F, Liu XY, Zhang YX, Dong F, Losic D (2016) Engineering of three dimensional (3-D) ?diatom@TiO_2?@MnO_2? composites with enhanced supercapacitor performance. Electrochim Acta 190:159–167. https://doi.org/10.1016/j.electacta.2015.12.178

Hao S-M, Qu J, Zhu Z-S, Zhang X-Y, Wang Q-Q, Yu Z-Z (2016) Hollow manganese silicate nanotubes with tunable secondary nanostructures as excellent Fenton-type catalysts for dye decomposition at ambient temperature. Adv Funct Mater 26:7334–7342. https://doi.org/10.1002/adfm.201603315

Jiang DB, Liu X, Xu X, Zhang YX (2018) Double-shell Fe_2O_3? hollow box-like structure for enhanced photo-Fenton degradation of malachite green dye. J Phys Chem Solids 112:209–215. https://doi.org/10.1016/j.jpcs.2017.09.033

Le QJ, Wang T, Tran DNH, Dong F, Zhang YX, Losic D (2017) Morphology-controlled MnO_2 modified silicon diatoms for high-performance asymmetric supercapacitors. J Mater Chem A 5:10856–10865. https://doi.org/10.1039/c6ta11210b

Lee C-S, Gong J, Huong CV, Oh D-S, Chang Y-S (2016) Macroporous alginate substrate-bound growth of Fe_0 nanoparticles with high redox activities for nitrate removal from aqueous solutions. Chem Eng J 298:206–213. https://doi.org/10.1016/j.cej.2016.03.113

Li F, Xing Y, Huang M, Li KL, Yu TT, Zhang YX, Losic D (2015) ?MnO_2? nanostructures with three-dimensional (3D) morphology replicated from diatoms for high-performance supercapacitors. J Mater Chem A 3:7855–7861. https://doi.org/10.1039/c5ta00634a

Ling Y, Gao Q, Ma C-F, Gong Y-S, Bo H, Xia K-S, Zhou C-G (2016) A waxberry-like SiO_2@$MnSiO_3$? core–shell nanocomposite synthesized via a simple solvothermal self-template method and its potential in catalytic degradation and heavy metal ion removal. RSC Adv 6:23360–23369. https://doi.org/10.1039/c6ra00070c

Liu S, Peng W, Sun H, Wang S (2014) Physical and chemical activation of reduced graphene oxide for enhanced adsorption and catalytic oxidation. Nano 6:766–771. https://doi.org/10.1039/c3nr04282k

Qu J, Li W, Cao CY, Yin XJ, Zhao L, Bai J, Qin Z, Song WG (2012) Metal silicate nanotubes with nanostructured walls as superb adsorbents for uranyl ions and lead ions in water. J Mater Chem 22:17222–17226. https://doi.org/10.1039/C2JM33178K

Shang J, Xie B, Li Y, Wei X, du N, Li H, Hou W, Zhang R (2016) Inflating strategy to form ultrathin hollow MnO_2 nanoballoons. ACS Nano 10:5916–5921. https://doi.org/10.1021/acsnano.6b01229

Subramanian G, Madras G (2016) Introducing saccharic acid as an efficient iron chelate to enhance photo-Fenton degradation of organic contaminants. Water Res 104:168–177. https://doi.org/10.1016/j.watres.2016.07.070

Tan X, Wan Y, Huang Y, He C, Zhang Z, He Z, Hu L, Zeng J, Shu D (2016) Three-dimensional MnO_2 porous hollow microspheres for enhanced activity as ozonation catalysts in degradation of bisphenol A. J Hazard Mater 321:162–172. https://doi.org/10.1016/j.jhazmat.2016.09.013

Ventura-Camargo Bde C, de Angelis Dde F, Marin-Morales MA (2016) Assessment of the cytotoxic, genotoxic and mutagenic effects of the commercial black dye in Allium cepa cells before and after bacterial biodegradation treatment. Chemosphere 161:325–332. https://doi.org/10.1016/j.chemosphere.2016.06.085

Xiao F, Li W, Fang L, Wang D (2016) Synthesis of akageneite (beta-FeOOH)/reduced graphene oxide nanocomposites for oxidative decomposition of 2-chlorophenol by Fenton-like reaction. J Hazard Mater 308:11–20. https://doi.org/10.1016/j.jhazmat.2016.01.011

Yec CC, Zeng HC (2014) Nanobubbles within a microbubble: synthesis and self-assembly of hollow manganese silicate and its metal-doped derivatives. ACS Nano 8:6407–6416. https://doi.org/10.1021/nn501948h

Yin J, Gao F, Wu Y, Wang J, Lu Q (2010) Synthesis of Mn_3O_4? octahedrons and other manganese-based nanostructures through a simple and green route. CrystEngComm 12:3401. https://doi.org/10.1039/c003551n

Yu F, Zhou H, Zhu Z, Sun J, He R, Bao J, Chen S, Ren Z (2017) Three-dimensional nanoporous iron nitride film as an efficient electrocatalyst for water oxidation. ACS Catal 7:2052–2057. https://doi.org/10.1021/acscatal.6b03132

Yuan W, Yuan P, Liu D, Deng L, Zhou J, Yu W, Chen F (2016) A hierarchically porous diatomite/silicalite-1 composite for benzene adsorption/desorption fabricated via a facile pre-modification in situ synthesis route. Chem Eng J 294:333–342. https://doi.org/10.1016/j.cej.2016.02.099

Zhan G, Yec CC, Zeng HC (2015) Mesoporous bubble-like manganese silicate as a versatile platform for design and synthesis of nanostructured catalysts. Chemistry 21:1882–1887. https://doi.org/10.1002/chem.201405697

Zhang L, Lian J, Wu L, Duan Z, Jiang J, Zhao L (2014a) Synthesis of a thin-layer MnO_2 nanosheet-coated Fe_3O_4? nanocomposite as a magnetically separable photocatalyst. Langmuir: ACS J Surf Colloids 30:7006–7013. https://doi.org/10.1021/la500726v

Zhang YX, Hao XD, Li F, Diao ZP, Guo ZY, Li J (2014b) pH-dependent degradation of methylene blue via rational-designed MnO_2 nanosheet-decorated diatomites. Ind Eng Chem Res 53:6966–6977. https://doi.org/10.1021/ie5002229

Zhang YX, Hao XD, Wang T, Meng YX, Han X (2014c) MnO(x)-modified ZnAl-LDOs as high-performance adsorbent for the removal of methyl orange. Dalton Trans 43:6667–6676. https://doi.org/10.1039/c3dt53597e

Zhang YX, Huang M, Li F, Wang XL, Wen ZQ (2014d) One-pot synthesis of hierarchical MnO_2-modified diatomites for electrochemical capacitor electrodes. J Power Sources 246:449–456. https://doi.org/10.1016/j.jpowsour.2013.07.115

Zhang AY, Lin T, He YY, Mou YX (2016a) Heterogeneous activation of H_2O_2? by defect-engineered $TiO_{(2-x)}$ single crystals for refractory pollutants degradation: a Fenton-like mechanism. J Hazard Mater 311:81–90. https://doi.org/10.1016/j.jhazmat.2016.02.071

Zhang H, Lin C, Han T, Du F, Zhao Y, Li X, Sun Y (2016b) Visualization of the formation and 3D porous structure of ag doped MnO_2 aerogel monoliths with high photocatalytic activity. ACS Sustain Chem Eng 4:6277–6287. https://doi.org/10.1021/acssuschemeng.6b00578

Zhang J, He T, Zhang W, Sheng J, Amiinu IS, Kou Z, Yang J, Mai L, Mu S (2016c) Na-Mn-O nanocrystals as a high capacity and long life anode material for Li-ion batteries. Adv Energy Mater 7:1602092. https://doi.org/10.1002/aenm.201602092

Zhu S, Li L, Liu J, Wang H, Wang T, Zhang Y, Zhang L, Ruoff RS, Dong F (2018) Structural directed growth of ultrathin parallel birnessite on beta-MnO_2 for high-performance asymmetric supercapacitors. ACS Nano 12:1033–1042. https://doi.org/10.1021/acsnano.7b03431